

Photoluminescence-free photoreflectance spectra using dual frequency modulation

J. Plaza

Departamento de Investigación, Centro de Investigación y Desarrollo de la Armada, Arturo Soria 289, 28033 Madrid, Spain

D. Ghita, J. L. Castaño, and B. J. Garcia^{a)}

Laboratorio de Electrónica y Semiconductores, Departamento de Física Aplicada, Universidad Autónoma de Madrid, 28049 Madrid, Spain

(Received 23 July 2007; accepted 9 September 2007; published online 5 November 2007)

Photoreflectance (PR) spectra are usually obtained by measuring the relative change on the reflectivity of a semiconducting sample induced by a chopped laser beam. The laser beam can also produce photoluminescence (PL) emission at the sample surface which, detected at its same frequency, could appear as an offset distorting the PR spectrum. This parasitic and intrinsically noisy PL signal, not easily discriminated electronically nor optically filtered, can become the dominant part of the PR spectrum at low sample temperatures, hiding spectrum features under its associated noise, or even avoiding data acquisition. An alternative method for PL signal discrimination is proposed in this work, using a different chopping frequency for each light beam: PL and reflected signals will appear each one at its own chopping frequency, while PR signal will be detected at its frequency sum, allowing signal separation by frequency. Both experimental setups are compared using a highly luminescent quantum well structure at low temperatures. While the standard setup suffers the PL limitation, the proposed method overcomes this constraint, allowing good quality spectra to be measured at temperatures as low as 12 K. © 2007 American Institute of Physics. [DOI: 10.1063/1.2802991]

I. INTRODUCTION

Photoreflectance (PR) is a contactless, nondestructive, and very sensitive optical modulation spectroscopy allowing the experimental determination of the energy of critical points in semiconductor samples.¹ A typical PR setup uses a monochromated lamp light beam to measure the reflected intensity at the surface of a semiconducting sample by means of a photodetector. A second beam, usually a laser with photon energy larger than the sample band gap, is pointed to overlap the first beam on the sample surface, producing electron-hole pairs that change the sample built-in field near the surface, and thus its reflectivity at wavelengths in the neighborhood of the sample critical points.^{2,3} The PR spectrum $P_R(\lambda)$, defined as the relative change on the sample reflectivity $R(\lambda)$ induced by the laser, is measured over the spectral range of interest. Under low electric field conditions, it is related to the dielectric function third derivative,⁴ allowing band gap determination by simple data fitting.

The spectrum of the reflected beam intensity $R_M(\lambda)$, as measured with a photodetector, depends on the spectral response of the lamp, monochromator, sample reflectivity, photodetector sensitivity, optics, and any other wavelength-dependent component used in the path of the lamp light. The laser induced change on the reflected intensity $\Delta R_M(\lambda)$ is proportional to the incident (or reflected) lamp intensity,

$$\Delta R_M(\lambda) = \alpha(\lambda) R_M(\lambda), \quad (1)$$

where the factor $\alpha(\lambda)$ also depends on the incident laser power density, kept constant during the experiment. The experimental PR spectrum, built as the ratio between the signals $\Delta R_M(\lambda)$ and $R_M(\lambda)$, is not sensitive to the above spectral responses because they are simultaneously present in both signals and then canceled when calculating the ratio

$$P_{RM}(\lambda) = \frac{\Delta R_M(\lambda)}{R_M(\lambda)} = \alpha(\lambda) = \frac{\Delta R(\lambda)}{R(\lambda)} = P_R(\lambda). \quad (2)$$

The measured and dimensionless PR spectrum should be independent of the experimental setup.

II. STANDARD PHOTOREFLECTANCE SETUP

Due to the small value of $P_R(\lambda)$, typically smaller than 10^{-3} , the experimental setup for PR acquisition uses a chopper on the laser path to produce a square wave modulation of the laser intensity with period T_0 and peak intensity I_0 . The sample reflectivity will change with the same chopping period and, assuming fast carrier generation-recombination processes, with the same time dependence, expressed as its Fourier series,

$$\Delta R_M(\lambda, t) = \Delta R_M(\lambda) \left[\frac{1}{2} + \frac{2}{\pi} \sum_{k=1,3,5,\dots}^{\infty} \frac{1}{k} \sin(k\omega_0 t) \right], \quad (3)$$

where $f_0 = (T_0)^{-1} = \omega_0 / 2\pi$ is its fundamental frequency. The photodetected signal $S_{PD}(\lambda, t)$ will have two terms:

^{a)}Electronic mail: basilio.javier.garcia@uam.es

$$S_{PD}(\lambda, t) = R_M(\lambda) + \Delta R_M(\lambda, t). \quad (4)$$

A dc voltmeter is used to measure R_M , while a lock-in amplifier measures the small ac rms value at f_0 , where the maximum amplitude $2\Delta R_M(\lambda)/\pi$ is available; PR spectra are built from the ac to dc ratio of the detected signal [Eq. (2)]. This PR signal can be delayed, relative to the laser excitation, by a different value at each spectrum feature or material layer in the sample, making $\Delta R_M(\lambda)$ and $P_{RM}(\lambda)$ phase sensitive. Dual phase lock-in amplifiers are then preferred in order to simultaneously measure both components of the ac signal (either x - y or R - θ). As the $P_{RM}(\lambda)$ data points are complex values, a further phase analysis can be done.⁵

However, an important problem occurs when the laser induces near-band-gap photoluminescence (PL) emission, appearing superimposed (wavelength integrated) to the reflected beam in the solid angle seen by the detector. The measured signal includes now the PL related term $P_L(t)$

$$S_{PD}(\lambda, t) = R_M(\lambda) + \Delta R_M(\lambda, t) + P_L(t). \quad (5)$$

Since, assuming again a negligible carrier lifetime, the $P_L(t)$ waveform will be also a square wave, the lock-in will not be able to separate it from the true PR signal. PL appears as a constant ac offset P_L added to $\Delta R_M(\lambda)$ that distorts the PR spectrum,

$$P_{RM}(\lambda) = \frac{\Delta R_M(\lambda) + P_L}{R_M(\lambda)} = P_R(\lambda) + \frac{P_L}{R_M(\lambda)}. \quad (6)$$

The experimentally obtained PR spectrum, $P_{RM}(\lambda)$, differs from the real one, $P_R(\lambda)$, by the last term, which should be removed to obtain a clean $P_{RM}(\lambda)$ with zero base line. The PL emission related offset, increasing as the sample temperature is decreased, could be several orders of magnitude larger than $\Delta R_M(\lambda)$, avoiding lock-in offset compensation, forcing to operate its electronics with low resolution before numerical offset subtraction, or even hiding $\Delta R_M(\lambda)$ under its noise.

Effectively, PL emission is intrinsically noisy because photon emission by electron-hole pairs is an independent process whose noise increases as $P_L^{1/2}$. Although its averaged value may be removed from the spectrum as it was said before, its amplitude noise would remain in the spectrum. The strong filtering required to remove this noise would make PR acquisition a large and time consuming task. Furthermore, sample cooling for PR measurements at low temperatures requires long times for sample thermal stabilization. A slight temperature fluctuation during PR acquisition could lead to a noticeable difference on PL emission in such a way that small temperature transients will appear as waves on the spectrum base line, distorting it and confusing data analysis.^{6,7}

III. DUAL FREQUENCY PHOTOREFLECTANCE SETUP

To overcome the problems related to the standard setup, we propose a dual frequency photoreflectance setup (DFPR), using a double sector chopper blade, each sector having a different number of slots, n_1 and n_2 . Setting the chopper blade spin frequency to f_0 , both light beams are chopped as

square waves with two different periods, $(n_1 f_0)^{-1}$ for the lamp beam $l(\lambda, t)$ and $(n_2 f_0)^{-1}$ for the laser beam $L(t)$, written as

$$l(\lambda, t) = l_0(\lambda) \left[\frac{1}{2} + \frac{2}{\pi} \sum_{k_1=1,3,5,\dots}^{\infty} \frac{1}{k_1} \sin(k_1 n_1 \omega_0 t) \right], \quad (7a)$$

$$L(t) = L_0 \left[\frac{1}{2} + \frac{2}{\pi} \sum_{k_2=1,3,5,\dots}^{\infty} \frac{1}{k_2} \sin(k_2 n_2 \omega_0 t) \right]. \quad (7b)$$

Using the DFPR setup, S_{PD} will have three terms, as given in Eq. (5), but R_M also depending on t ,

$$S_{PD}(\lambda, t) = R_M(\lambda, t) + \Delta R_M(\lambda, t) + P_L(t). \quad (8)$$

The reflected light and the PL contribution excited by the laser beam are therefore

$$R_M(\lambda, t) = R_M(\lambda) \left[\frac{1}{2} + \frac{2}{\pi} \sum_{k_1=1,3,5,\dots}^{\infty} \frac{1}{k_1} \sin(k_1 n_1 \omega_0 t) \right], \quad (9a)$$

$$P_L(t) = P_L \left[\frac{1}{2} + \frac{2}{\pi} \sum_{k_2=1,3,5,\dots}^{\infty} \frac{1}{k_2} \sin(k_2 n_2 \omega_0 t) \right]. \quad (9b)$$

Since the reflected beam intensity change induced by the laser is only produced and detected when both beams illuminate simultaneously the sample surface, Eq. (1) should now be written as

$$\begin{aligned} \Delta R_M(\lambda, t) &= \alpha(\lambda) R_M(\lambda, t) \frac{L(t)}{L_0} \\ &= \alpha(\lambda) R_M(\lambda) \left(\frac{1}{4} + \frac{1}{\pi} \sum_{k_1=1,3,5,\dots}^{\infty} \frac{1}{k_1} \sin(k_1 n_1 \omega_0 t) \right. \\ &\quad + \frac{1}{\pi} \sum_{k_2=1,3,5,\dots}^{\infty} \frac{1}{k_2} \sin(k_2 n_2 \omega_0 t) \\ &\quad + \frac{2}{\pi^2} \sum_{k_1, k_2 \text{ odds}} \frac{1}{k_1 k_2} \{ \cos[(k_2 n_2 - k_1 n_1) \omega_0 t] \\ &\quad \left. - \cos[(k_2 n_2 + k_1 n_1) \omega_0 t] \} \right). \end{aligned} \quad (10)$$

It can be seen from the above equations that, in addition to the dc components, $P_L(t)$ has components at frequencies given by $k_2 n_2 f_0$, while $R_M(t)$ will be observed at frequencies $k_1 n_1 f_0$. On the other hand, $\Delta R_M(t)$, being the product of two series, will appear not only at the same frequencies as P_L and R_M (with a much smaller amplitude than this one) but also at any other having the forms $(k_2 n_2 + k_1 n_1) f_0$ or $|k_2 n_2 - k_1 n_1| f_0$. Provided that n_2 and n_1 have no common dividers, to avoid mixing different terms, the larger amplitude terms of $\Delta R_M(t)$ will appear for $k_1 = k_2 = 1$ at $f = (n_2 + n_1) f_0$ and $f = |n_2 - n_1| f_0$, both with the same amplitude given by $2\alpha(\lambda) R_M(\lambda) / \pi^2$.

The solid line in Fig. 1 shows the frequency spectrum, obtained as the fast Fourier transform (FFT), of a simulated S_{PD} signal as given by Eqs. (7)–(10) using $n_1 = 7$, $n_2 = 5$, and $f_0 = 100$ Hz (later used for the experiments), with amplitudes

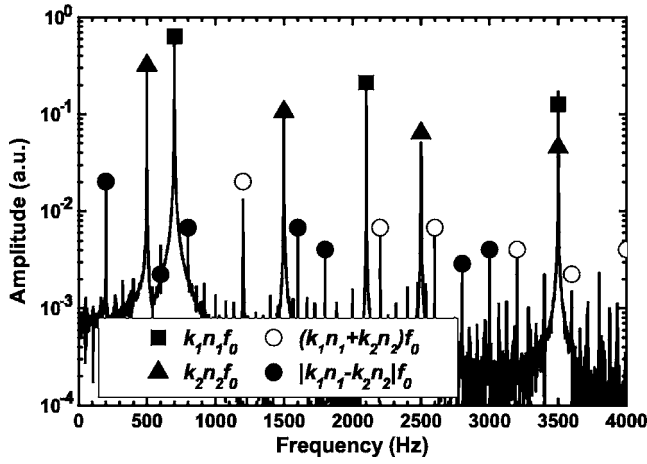


FIG. 1. Solid line: frequency spectrum of a numerically simulated DFPR signal; symbols indicate the source and amplitude of some main harmonics.

given by $R_M=1$, $\alpha=0.1$, and $P_L=0.5$. The dominant harmonic series at $700k_1$ Hz and $500k_2$ Hz, belonging to the R_M and P_L signals, respectively, can be clearly seen in this figure. Although the useful frequencies for ΔR_M detection are spread over the frequency axis, the larger amplitudes are observed at 200 and 1200 Hz, clearly detached from the other series. The proposed DFPR procedure is based on the simultaneous measurement, choosing the frequencies with the larger amplitude available, of ΔR_M [at either $f=(n_2+n_1)f_0$ or $f=|n_2-n_1|f_0$] and R_M (at $f=n_1f_0$, including a negligible $\Delta R_M/2$ contribution), to build the PR spectrum as given by Eq. (2), avoiding the PL interference due to the above frequency separation.

IV. EXPERIMENT

In order to compare the quality of the spectra taken using each setup, we used the same test sample, including an 8 nm $\text{Ga}_{0.8}\text{In}_{0.2}\text{As}$ quantum well (QW) surrounded by two 250 nm $\text{Ga}_{0.9}\text{In}_{0.1}\text{As}$ barriers, with a final 25 nm GaAs capping layer. The sample was grown, unintentionally doped, on a semi-insulating GaAs (001) substrate by chemical beam epitaxy using tertiarybutylarsine, triethylgallium, and trimethylindium as precursors.^{6,8,9} The light of a 100 W tungsten lamp was dispersed by a grating monochromator and detected, after reflecting on the sample surface, by a GaInAs photodetector. An Ar^+ laser was chopped at $f_0=100$ Hz during PR measurements by using a chopper with either a single ten-slot blade or a dual sector blade with five and seven slots. A dual frequency–dual phase lock-in amplifier was used for data acquisition in the dual frequency setup (R_M detected at 700 Hz and ΔR_M at 1200 Hz), while a voltmeter was used for single frequency measurements combined with the same lock-in (R_M detected at dc and ΔR_M at 1000 Hz). The whole spectra could be phase rotated after acquisition to search for its maximum amplitude. Samples were introduced in a closed cycle He cryostat allowing temperature control between 12 K and room temperature. The above PR setup, as used in our laboratory, can be easily modified to allow the acquisition of PL spectra, whose emission peaks will be compared to the PR spectra features.

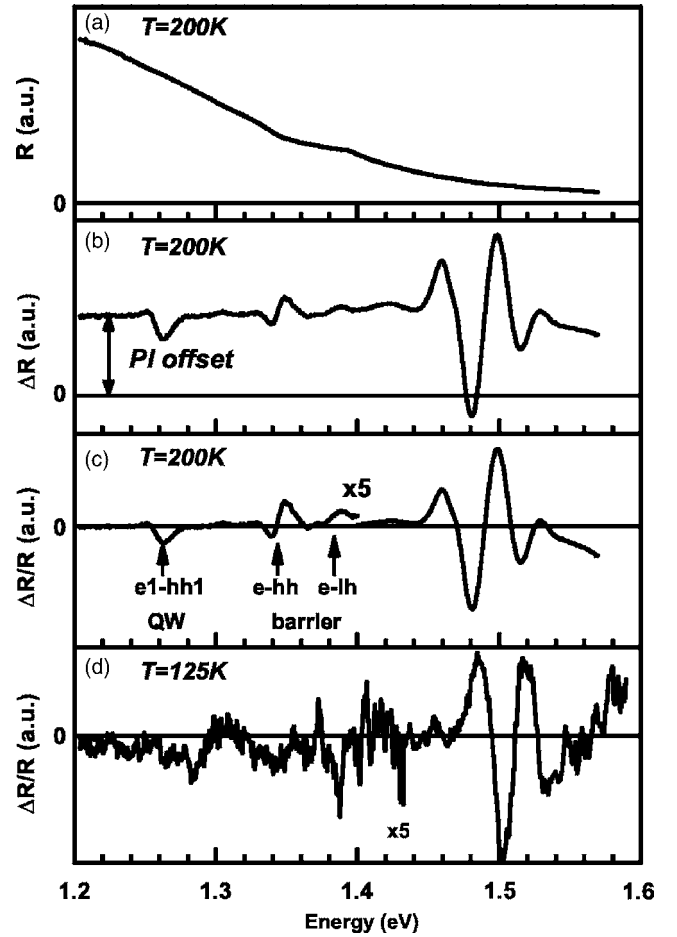


FIG. 2. PR data of the test sample, as obtained using the single frequency setup at $T=200$ K, showing (a) $R_M(\lambda)$, (b) $\Delta R_M(\lambda)$, and (c) $P_{RM}(\lambda)$ obtained after PL offset removal. PR spectrum quality is degraded at lower temperatures, as shown in (d) for $T=125$ K.

V. RESULTS AND DISCUSSION

Test sample spectra $R_M(\lambda)$ and $\Delta R_M(\lambda)$, measured at 200 K using the classical single frequency setup, are shown in Figs. 2(a) and 2(b). The offset in $\Delta R_M(\lambda)$ due to PL emission can be observed, being negligible at much higher temperatures. Also shown in Fig. 2(c) is the calculated $P_{RM}(\lambda)$ spectrum after offset correction, showing that, under moderate PL emission, PR acquisition can be done with the standard setup. The larger peaks at about 1.48 eV are associated with the GaAs layers (substrate, buffer layer, and capping layer), while the second peak group in amplitude is related to the $\text{Ga}_{0.9}\text{In}_{0.1}\text{As}$ barrier band gap, showing a clear valence band splitting due to the biaxial strain (e-hh at 1.345 eV and e-lh at 1.381 eV), as it is suggested by the Kramers-Kronig analysis of the spectrum.¹⁰ The third, low-energy and low amplitude peak (at 1.263 eV) is related to the $\text{Ga}_{0.8}\text{In}_{0.2}\text{As}$ QW fundamental transition (e1-hh1). Some weak features are observed between the last two groups, which could be assigned to other energy levels in the QW.

As the sample temperature is further reduced, the observed offset in $\Delta R_M(\lambda)$ increases, resulting in a noisy $P_{RM}(\lambda)$ spectrum even after offset correction, as it can be seen in Fig. 2(d) at 125 K, where the small features start to be masked by noise. At much lower temperatures, spectra are useless.

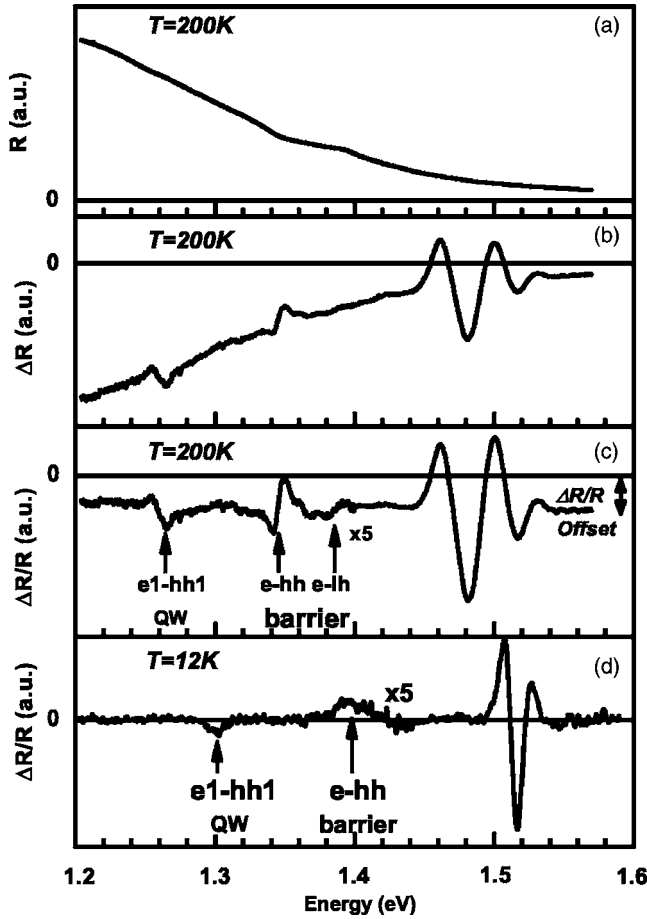


FIG. 3. PR data of the test sample, as obtained using the dual frequency setup at $T=200$ K, showing (a) $R_M(\lambda)$, (b) $\Delta R_M(\lambda)$, and (c) $P_{RM}(\lambda)$ without offset removal. PR spectrum quality is maintained at lower temperatures, as shown in (d) for $T=12$ K (offset removed).

Spectra of the same sample at 200 K, taken using the DFPR setup, are shown in Figs. 3(a)–3(c). No noticeable difference could be observed in the $R_M(\lambda)$ spectrum [Fig. 3(a)]. Concerning the $\Delta R_M(\lambda)$ spectrum shown in Fig. 3(b), it shows an unexpected profile: a signal has been added to the typical PR signal, whose shape looks like a $R_M(\lambda)$ spectrum replica with a scale factor $\beta < 0$. The calculated $P_{RM}(\lambda)$ from the above data, seen in Fig. 3(c), shows a clear constant offset β with constant phase, since PR spectrum has been built on the form

$$P_{RM}(\lambda) = \frac{\Delta R_M(\lambda) + \beta R_M(\lambda)}{R_M(\lambda)} = P_R(\lambda) + \beta. \quad (11)$$

This unexpected behavior is associated with small chopper blade manufacturing defects. The frequency spectrum of a light source chopped by an imperfect n -slot blade turning at a frequency f_0 includes not only the main harmonics at knf_0 ($k=1,3,5,\dots$) but also small components at mf_0 ($m=1,2,3,\dots$). This effect can be numerically simulated, but instead of showing this simulation, we have preferred to measure this effect by chopping a light-emitting diode (LED) beam with the same $n=7$ slot chopper blade used for DFPR at $f_0=100$ Hz. The LED was battery powered to avoid harmonic propagation from the power supply at 50 or 100 Hz. The FFT of this signal, as calculated by an oscilloscope, is

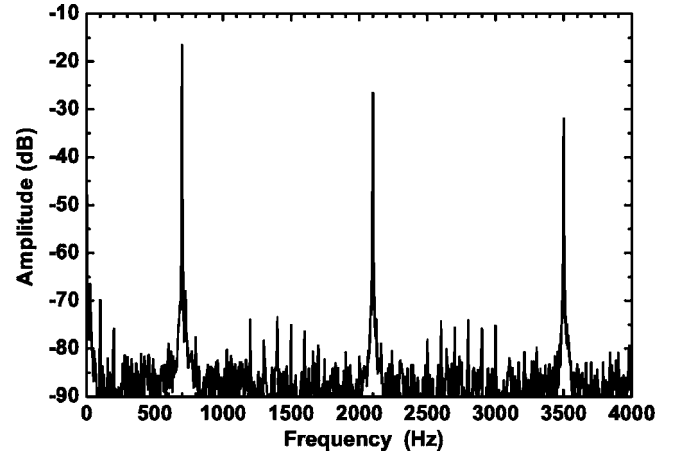


FIG. 4. Frequency spectrum of a battery powered LED chopped through the outer sector of a seven-slot blade spinning at 100 Hz. Spurious harmonics at 100m Hz ($m=1,2,3,\dots$) clearly propagate through the entire spectrum.

shown in Fig. 4. The first three harmonics ($k=1, 3$, and 5) of the square wave are dominant in the spectrum, but the presence of small spurious harmonics at frequencies of (100m) Hz ($m=1,2,3,\dots$) can be clearly seen in this figure. The 1200 Hz harmonic, responsible for the propagation of the lamp light from its 700 Hz frequency during DFPR, is one of them; its amplitude is about 60 dB ($|\beta| \approx 10^{-3}$) below the main $k=1$ value. This value is in good agreement with the maximum obtained value (by phase rotation) of the $P_{RM}(\lambda)$ spectrum base line offset β , which confirms the given explanation of this effect. It is important to notice that this offset is observed as constant on a day-to-day basis in the PR acquisition system, being easily removed after data acquisition.

A similar result, not shown here, could be observed using the $n=5$ blade, allowing PL propagation to the measured $\Delta R_M(\lambda)$ spectrum. This PL signal harmonic propagation with its own and similar attenuation $|\beta'| \approx 10^{-3}$ could also be observed in this high PL-efficient sample under very high laser excitation power, giving rise to a PR spectrum of the form

$$\begin{aligned} P_{RM}(\lambda) &= \frac{\Delta R_M(\lambda) + \beta R_M(\lambda) + \beta' P_L}{R_M(\lambda)} \\ &= P_R(\lambda) + \beta + \beta' \frac{P_L}{R_M(\lambda)}. \end{aligned} \quad (12)$$

When simultaneous contamination by both signals takes place, the last term of the small PL propagated signal ($\beta' P_L$) should be first subtracted from the signal detected at the frequency sum, as it was done for the single frequency measurements. After PL removal, $P_R(\lambda)$ spectrum can be calculated and the remaining offset β subtracted. The DFTR setup allows PL-free PR measurements at low temperatures under moderate laser power modulation, as it is shown in Fig. 3(d), where the PR spectrum of the test sample, taken at $T=12$ K, is reproduced. Because carrier freezing at low temperatures, observed by other authors,^{7,11} does not affect the spectrum intensity, even the weak QW signal is clearly seen in the 10^{-5} range, not masked by the PL signal nor by its associated noise, allowing critical point energy determination

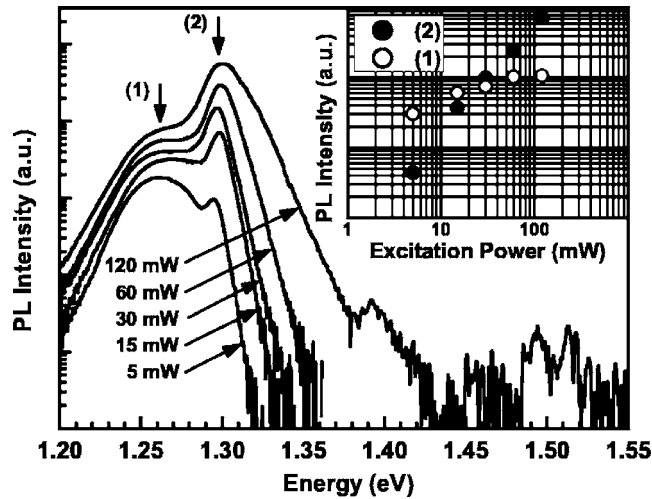


FIG. 5. PL spectra of the test sample at $T=12$ K for laser excitation powers ranging from 5 to 120 mW. Shown in the inset is the plot of the integrated intensity vs laser excitation power for peaks labeled (1) and (2).

under strong luminescence emission. Clear features close to the energies of 1.3 and 1.4 eV are observed in the 12 K DFPR spectrum, associated with the $\text{Ga}_{0.8}\text{In}_{0.2}\text{As}$ QW fundamental transition ($e1\text{-}hh1$) and to the $e\text{-}hh$ subband of the $\text{Ga}_{0.9}\text{In}_{0.1}\text{As}$ barrier.

In order to confirm the above PR feature identification, PL spectra of the same sample were measured at $T=12$ K for different laser excitation power values. The obtained PL spectra are shown in Fig. 5 (note the logarithmic scale), where two main PL peaks can be observed at 1.263 and 1.296 eV. The integrated intensity dependence versus excitation power for both peaks, also shown in the inset of Fig. 5, is very different. While the first and wider peak saturates its intensity when increasing the laser excitation power, indicating that it is impurity related, the intensity dependence of the second and sharper peak is superlinear, showing its excitonic character.

From the above observations, the second peak at 1.295 eV should be the excitonic $e1\text{-}hh1$ QW transition, in good agreement with the PR obtained energy, which shows a small Stokes shift. The peak at 1.263 eV can be identified as an electron to carbon acceptor recombination transition in the QW ($e1\text{-}C^0$) due to the residual carbon doping introduced during growth, as it is usually observed on samples grown by chemical beam epitaxy; the high radiative recombination efficiency of this impurity makes it visible in PL spectra even for low carbon concentrations, while its binding energy (about 33–36 meV from Fig. 5) is very close to the carbon acceptor binding energy in bulk GaAs (29 meV).

Also observed in the PL spectrum for the higher laser excitation power, emerging over the noise level, is a small peak at 1.393 eV which could be related to the $e\text{-}hh$ recombination in the $\text{Ga}_{0.9}\text{In}_{0.1}\text{As}$ barrier, also in good agreement with the DFPR obtained energy. Even GaAs buffer layer related small peaks in the 1.5 eV region can be identified in the same PL spectrum, related to the $e\text{-}C^0$ and excitonic transitions.

VI. CONCLUSIONS

We have proposed an alternative setup for PR measurements, named DFPR, preventing spectrum distortion by PL signal, using a dual sector chopper blade with different numbers of slots to chop the lamp and laser beams at different frequencies. The photodetected signal includes different contributions separated in the frequency domain that are detected by a dual frequency lock-in. Extremely high quality chopper blades should be used to avoid signal mixing due to spurious harmonic propagation and its associated data treatment. We have been able to obtain good quality PR spectra in a highly luminescent sample at 12 K using the DFPR method, overcoming the limitations of the standard setup and showing that photoreflectance technique can be efficiently used for semiconductor band gap determination at low temperatures. DFPR spectra have been compared with PL spectra, showing good agreement between their corresponding peak energies at 12 K.

ACKNOWLEDGMENTS

This work has been supported by the Spanish Ministry of Education and Science under Project Nos. MAT2003-07841 and TEC2007-65892/MIC.

- ¹M. Cardona, *Modulation Spectroscopy* (Academic, New York, 1969).
- ²R. E. Nahory and J. L. Shay, *Phys. Rev. Lett.* **21**, 1569 (1968).
- ³N. Bottka, D. K. Gaskill, R. S. Sillmon, R. Henry, and R. Glosser, *J. Electron. Mater.* **17**, 161 (1987).
- ⁴D. E. Aspnes, *Surf. Sci.* **37**, 418 (1973).
- ⁵A. V. Ganzha, R. V. Kus'menko, W. Kircher, J. Schreiber, and S. Hildebrandt, *Semiconductors* **32**, 245 (1998).
- ⁶J. Plaza, J. L. Castaño, B. J. García, H. Carrère, and E. Bedel-Pereira, *Appl. Phys. Lett.* **86**, 121918 (2005).
- ⁷K. I. Lin and J. S. Hwang, *Appl. Phys. Lett.* **89**, 192116 (2006).
- ⁸M. Aït-Lhouss, J. L. Castaño, B. J. García, and J. Piqueras, *J. Appl. Phys.* **78**, 5834 (1995).
- ⁹D. Wildt, B. J. García, J. L. Castaño, and J. Piqueras, *J. Vac. Sci. Technol. B* **16**, 1804 (1998).
- ¹⁰T. J. C. Hosea, *Phys. Status Solidi B* **182**, K43 (1994).
- ¹¹T. Mishima, M. Miura, S. Ozaki, and S. Adachi, *J. Appl. Phys.* **91**, 4904 (2002).